ACS APPLIED MATERIALS & INTERFACES

www.acsami.org

Research Article

Quenching Thermal Transport in Aperiodic Superlattices: A Molecular Dynamics and Machine Learning Study

Pranay Chakraborty, Yida Liu, Tengfei Ma, Xixi Guo, Lei Cao, Run Hu,* and Yan Wang*

Cite This: *ACS Appl. Mater. Interfaces* 2020, 12, 8795−8804

Read Online

ACCESS | Metrics & More | Article Recommendations

ABSTRACT: Random multilayer (RML) structures, or aperiodic superlattices, can localize coherent phonons and therefore exhibit drastically reduced lattice thermal conductivity compared to their superlattice counterparts. The optimization of RML structures is essential for obtaining ultralow thermal conductivity, which is critical for various applications such as thermoelectrics and thermal barrier coatings. A higher degree of disorder in RMLs will lead to stronger phonon localization and, correspondingly, a lower lattice thermal conductivity. In this work, we identified several essential parameters for quantifying the disorder in layer thicknesses of RMLs. We were able to correlate these disorder parameters with thermal conductivity, as confirmed by classical molecular dynamics simulations of conceptual Lennard-Jones RMLs. Moreover, we have shown that these parameters are effective as features for physics-based machine learning models to predict the lattice thermal conductivity of RMLs with improved accuracy and efficiency.

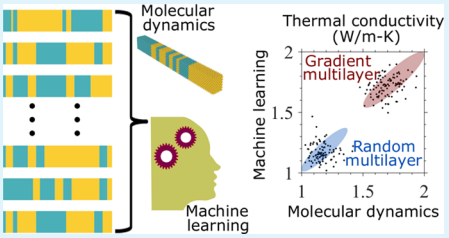

KEYWORDS: *superlattice, random multilayer, localization, disorder, lattice thermal conductivity, molecular dynamics, machine learning*

1. INTRODUCTION

Materials with an ultralow lattice thermal conductivity have always been of great interest to industry and governmental agencies. For example, thermal barrier coatings play a critical role in the automotive industry, the aerospace industry, and the space missions of the National Aeronautics and Space Administration (NASA). They are typically composed of materials with ultralow thermal conductivity and thus can protect the hot-side wall of an internal combustion engine from overheating, thereby enabling the use of a higher engine temperature for increased efficiency and lower emission.[1−3] For thermal barrier coatings, a lower thermal conductivity is almost always beneficial to their performance. Likewise, reducing the lattice thermal conductivity (κ_L) is one of the most effective ways for improving the figure-of-merit (ZT) of thermoelectric (TE) materials.[4−7] In fact, the low energy efficiency (≤10%) of existing TE materials prevents their vast application in various scenarios. It has been estimated that the ZT of TE materials should exceed 3 to compete with conventional power generators for converting heat into electricity; similarly, it should exceed this value for TE devices to replace conventional coolers for cooling purposes.[8] It is worth noting that the low efficiency of the high-temperature TE materials (e.g., LaTe and PrTe alloys) used in NASA's radioisotope thermoelectric generators renders it necessary to carry enormous ^{238}Pu, which is extremely scarce[9] and could cause atmospheric radioactive contamination due to the unwanted occurrence of launching or re-entry accidents,[10] to generate sufficient power in deep space missions. To attain the best outcome of TE technology, using TE materials with high conversion efficiency is of utmost importance. The efficiency of TE materials is measured by the dimensionless ZT, which is defined as

$$\mathrm{ZT} = \frac{\sigma S^2 T}{\kappa_e + \kappa_L} \quad (1)$$

where σ is the electrical conductivity, S is the Seebeck coefficient, T is the absolute temperature, and κ_e and κ_L are the electronic and lattice thermal conductivity, respectively. Since σ and κ_e are highly coupled via the Wiedemann−Franz law, it is obvious that a low κ_L is essential for achieving a high ZT without proportionally sacrificing the electrical properties of the crystalline materials. Besides, lowering the cross-plane κ_L results in a higher anisotropy of the thermal conductivity tensor, which is essential for applications like heat-assisted magnetic recording.[11]

Strategies for reducing κ_L have been extensively explored over the past few decades. Hicks and Dresselhaus are the two pioneers who revealed that 1D and 2D nanostructures exhibit significantly lower κ_L than their conventional 3D counterparts.[12,13] Since then, numerous strategies[14−17] have focused on combining various phonon scattering mechanisms, such as

Received: October 5, 2019
Accepted: January 29, 2020
Published: January 29, 2020

https://dx.doi.org/10.1021/acsami.9b18084
ACS Appl. Mater. Interfaces 2020, 12, 8795−8804

grain boundaries, embedded nanoparticles, and nanocomposites. These strategies hold great promise for balanced performance, reliability, cost, and complexity for manufacturing.[6,18] Indeed, nanocomposites/nanocrystals with grain-boundary scattering,[18,19] superlattices (SL) with interface scattering,[20] alloys with mass/bond-difference scattering,[21] and nanowires with boundary roughness scattering[14] have been reported to exhibit significantly lower κ_L compared to the bulk materials. However, it has become extremely challenging to reduce the κ_L of state-of-the-art materials further by merely engineering phonon scattering, which prevents the continued improvement of thermal barrier coatings and TE materials.

Recently, it has been revealed that random multilayer (RML) structures, also referred as aperiodic superlattice in literatures[22−24] (which is obtained by randomizing the layer thickness of a SL and maintaining the same average layer thickness and interface density as that of SL), exhibit significantly lower κ_L than their SL counterparts[22,24] and the κ_L of RMLs can even beat the random alloy limit. SL and RML are the two forms of multilayered structures that have gained significant interest among scientists and researchers, not just for their lower κ_L for thermal and thermoelectric applications. In fact, SLs and RMLs have been extensively explored to tailor their electronic and photonic transport properties for a wide range of applications, including photonic and optoelectronic devices.[25−29]

Depending on the period length, phonon can transmit either coherently or incoherently in SLs. It is well known that coherent phonons tend to have a long wavelength and mean free path, and incoherent phonons usually have a short wavelength and mean free path.[22,30] Since the coherent phonon modes are mostly localized in RMLs, RMLs exhibit a significantly lower cross-plane κ_L than their SL counterparts. Specifically, localization in RMLs results from the destructive interference of coherent phonons and has been reported to quench the phonon transport in both conceptual and realistic RML systems drastically. In particular, it was reported that an RML can exhibit up to 98% lower κ_L compared to that of the corresponding SL.[11,22,24,30] In addition, it was found that the κ_L of RMLs can be reduced even further by introducing lattice imperfections, for example, through doping.[30] Specifically, it was shown through molecular dynamics (MD) simulations that doping RMLs with foreign elements with significantly higher or lower characteristic vibrational frequency compared to that of base constituent materials can further reduce the κ_L of a conceptual RML by as much as ∼65%.[30] With a view to optimizing the RML structures to attain the lowest possible κ_L, Wang et al. investigated the thermal transport in SLs and RMLs with different interface conditions, average period thicknesses, bond strengths, and atomic masses, and reached certain pragmatic conclusions.[11,30] For example, for a fixed device length, it is more beneficial to use the smallest possible period length for lowering the κ_L of RMLs because a high interface density enhances the scattering of incoherent phonons. Since RMLs localize coherent phonons and the higher interface density reduces incoherent phonon transport, the overall κ_L of RMLs is significantly reduced. However, there still lacks a rigorous consideration of randomness in RMLs.

One important question would be how to define the randomness of an RML and relate the randomness with κ_L of RMLs quantitatively. This problem has two essential aspects. First, there are numerous possible RMLs with the same L (length) and same d (mean layer thickness) but different thickness distributions, which have different thermal conductivities; we want to find the best thickness distribution that leads to the lowest κ_L. Second, there are numerous possible arrangements (i.e., order of layers) for a given thickness distribution. To be more specific, there are up to $N! \times N!$ possible configurations of N-period RMLs. For example, a 16-period RML would have a maximum of $\sim 4.38 \times 10^{26}$ possible configurations. It is not practically possible to evaluate each of the arrangements using MD simulation or experiment to find the best configuration that will exhibit the lowest κ_L.

In a pioneering study by Ju et al.[31] in 2017, the atomistic Green's function (AGF) method was combined with Bayesian optimization to successfully minimize the thermal conductance of Si/Ge multilayers, demonstrating the effectiveness of material informatics in designing multilayered nanostructures. It is worth noting that the neglect of anharmonic phonon scatterings in the harmonic AGF approach used in Ju et al.'s work limits the generality of the conclusion to systems with strong anharmonicity—which is generally the case for thermoelectric materials—or high temperatures. In contrast, despite of its drawback in its inability to consider quantum phonon statistics at sub-Debye temperature and high computational costs, molecular dynamics can model anharmonic phonon scattering and thus phase breaking dynamics. Therefore, a molecular dynamics-based study will be important for testing the effectiveness of machine learning techniques for predicting thermal conductivity in those complex scenarios. In 2019, Juntunen et al. used the disorder limit, D (maximum deviation from the mean layer thickness d), to show the correlation between the degree of disorder and thermal conductivity of Si/Ge RMLs.[24] The authors reported that higher D results in lower κ_L. However, we can obviously obtain numerous RML structures with different thickness distributions that will have the same D, thus D itself is far from being sufficient to correlate the degree of randomness and κ_L of RMLs.

In this work, we identify two randomness parameters—the thickness-based index of randomization and period-based index of randomization to quantify the disorder in the layer/period thickness of RMLs. We further demonstrate in our work that machine learning (ML) is useful for identifying the optimal configuration of RML with the lowest κ_L because ML could significantly reduce the computational cost while retaining acceptable accuracy compared with pure molecular dynamics simulations.

2. METHODOLOGY

In this section, we first provide details of the nonequilibrium MD approach for calculating the κ_L and transmission spectra of multilayer structures. Then, we describe the machine learning approach for predicting κ_L, which is trained by MD results.

2.1. Molecular Dynamics Simulations. We conduct classical MD simulations to calculate the κ_L of the structures shown in Figure 1 with a view to relating the degree of randomness of the RML structures with their κ_L's. The structures for MD simulations are composed of two types of conceptual atoms A and B with atomic mass values of m_A = 40 g/mol and m_B = 90 g/mol, respectively. The interaction between the atoms is modeled using the Lennard-Jones (LJ) potential

https://dx.doi.org/10.1021/acsami.9b18084
ACS Appl. Mater. Interfaces 2020, 12, 8795−8804

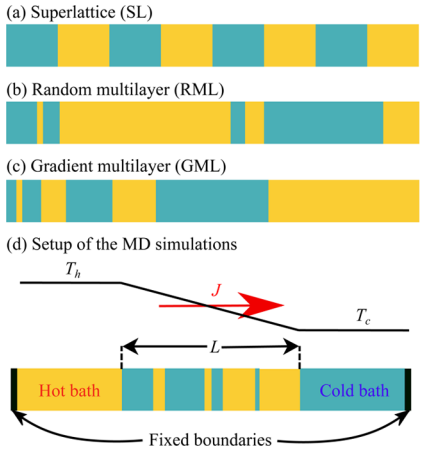

Figure 1. Schematic of the structures simulated in this work: (a) superlattice (SL), (b) random multilayer (RML), and (c) gradient multilayer (GML). Cyan and golden regions are composed of A- and B-type atoms, respectively. (d) Schematic of the nonequilibrium MD simulation setup. The black region signifies the fixed atoms during the simulation in the NVE ensemble.

$$\phi(r_{ij}) = 4\epsilon\left[\left(\frac{r_o}{r_{ij}}\right)^{12} - \left(\frac{r_o}{r_{ij}}\right)^{6}\right] \quad (2)$$

where $\phi(r_{ij})$ is the pairwise interaction energy, r_{ij} is the distance between atoms i and j, ϵ is the potential well depth, and r_o is the zero-potential-energy pair separation. We set the parameters of the LJ potential to be ϵ = 0.1664 eV and r_o = 0.34 nm. The cutoff radius for truncating the atomic interactions in MD simulation is set to be $r_c = 2.5r_o$. We choose to use the LJ potential for the computation because it has proven to be very effective for revealing the essential physics of phonon transport and localization,[11,32,33] and it is computationally more viable than the complex potentials like the Tersoff potential. The RML structures are created by replicating the conventional fcc unit cell (UC) of solid argon with a lattice constant of 5.23 Å in all three dimensions. The random thicknesses of RML structures considered in our study are generated by adopting the algorithm in ref 11 unless otherwise stated, and we ensure that the average layer thickness of the RMLs is the same as that of the corresponding SL.

In addition, we study the κ_L of the corresponding SL and gradient multilayer (GML) structures. It is worth noting that GMLs have the same thickness distribution as RMLs, but the layer thickness is arranged in an ascending order. For each of the RML configurations, a corresponding GML is created by sorting the layer thickness of the RML in ascending order. Based on the randomness, the SL, RML, and GML can be considered as uniform, random, and pseudorandom multilayered structures, respectively.

In Figure 1d, we show the MD simulation setup used in our study. The device (the structure of interest) is sandwiched between two sufficiently long (62 UC ≈ 327 Å) heat baths. We observed in our previous study that the heat bath should be long enough to obtain the converged values of κ_L from nonequilibrium MD simulations.[22] Hot and cold baths are composed of B- and A-type atoms, respectively. We use A_c = 4 UC × 4 UC as the cross-sectional area for our study. The simulation time step is chosen as Δt = 1 fs. At the beginning of the simulation, we apply the periodic boundary condition in all three dimensions and assign each atom with a random velocity following the Gaussian distribution such that the average kinetic energy of the atoms corresponds to a temperature of 5 K. Then, the simulation domain temperature is gradually raised from T = 5 to 30 K to ensure structural and thermodynamic stability. Subsequently, the entire simulation domain is relaxed in the isothermal-isobaric ensemble at zero pressure and a temperature of 30 K for 200 ps. To ensure that there is no cross-boundary energy transfer between the two ends of the simulation domain, we then apply the fixed boundary condition to the heat flow direction. In particular, we freeze an ∼1 nm-thick layer of atoms at both ends of the simulation domain. We conduct further simulation in the microcanonical (NVE) ensemble, that is, with a constant particle number N, constant volume V, and constant total energy E, for 25 ns. The hot and cold baths are maintained at temperatures of T_h = 33 K and T_c = 27 K, respectively, using a simple but effective velocity rescaling algorithm implemented in LAMMPS.[34] It is worth noting that a temperature bias of 6 K is chosen to avoid nonlinear effects near the heat bath and ensure a large signal-to-noise ratio. The lattice thermal conductivity is calculated as $\kappa_L = JL/[A_c(T_h - T_c)]$ where J is the heat current and A_c and L are the cross-sectional area and device length, respectively. The heat current is calculated as $J = \left(\frac{dE_h}{dt} + \frac{dE_c}{dt}\right)/2$ in which E_h and E_c are the kinetic energies that have been added to or subtracted from the hot and cold bath by the time t. Once the system reaches the steady state, we fit the $E_h - t$ and $E_c - t$ curves using the linear least regression method to obtain J. We use LAMMPS to conduct MD simulations.[34]

2.2. Transmission Calculation. The method developed by Sääskilahti et al.[35] was used to obtain phonon transmission spectra from nonequilibrium molecular dynamics simulations. Specifically, we choose an imaginary interface at approximately the center of the device and trace the velocity of atoms within 1 nm regions on the left and right side of the interface. We record the velocity data for 1 ns after the heat current across the devices is steady, that is, the system reaches the steady state. We calculate the harmonic force constants by tracking the change of potential energy as we displace the atoms slightly from their equilibrium positions. Finally, we are able to calculate the phonon transmission using the following equation

$$\tau(\omega) = -\frac{2}{t\omega k_B \Delta T}\sum_{i\in L, j\in R}\sum_{\alpha,\beta\in x,y,z}\mathrm{Im}\langle v_i^{\alpha}(\omega) \times K_{ij}^{\alpha\beta}(\omega)v_j^{\beta}(\omega)\rangle \quad (3)$$

where t is the simulation time, ω is the frequency, v_i^{α} is the Fourier transformed atomic velocity of atom i in the α direction, $K_{ij}^{\alpha\beta}$ is the harmonic force constant, and k_B is the Boltzmann constant. L and R denote the left and right side of the interface, respectively. More details of the transmission calculation can be found in Sääskilahti et al.'s original work.[35]

2.3. Machine Learning. The crucial step for ML-based predictions is to find the essential features for training and testing the model. Poor selection of features would make the model occupied with useless information and therefore will lead to a poor prediction of κ_L. For a physics-based ML problem like ours, finding the essential features becomes an even more complex and nontrivial job. In our study, the mass and binding energy mismatch of the constituent materials, thickness distributions, and thickness arrangements of the

https://dx.doi.org/10.1021/acsami.9b18084
ACS Appl. Mater. Interfaces 2020, 12, 8795−8804

RMLs are some of the crucial parameters that define the κ_L of RMLs. However, we choose to use the same constituent base materials and interaction energy to study the structural randomness of RMLs. It can be easily recognized that the structural parameters, for example, thickness distribution and thickness arrangement, are the main information that need to be fed into our ML model to obtain the best prediction of κ_L. To find out the best way of feeding the structural information to the ML model, we test different combinations of features that include thickness arrangements, the thickness-based index of randomization (R_d), the period-based index of randomization (R_p), and standard deviation of the thickness (δ). We provide the detailed definitions of R_d, R_p, and δ in Section 3.1. The performance of these features in an ML model is discussed in Section 3.3.

Considering the nonlinearity of our problem, we choose to predict the κ_L of RMLs employing a neural network (NN)-based ML model. A schematic of the NN model used in this work is provided in Figure 2. The number of hidden layers and

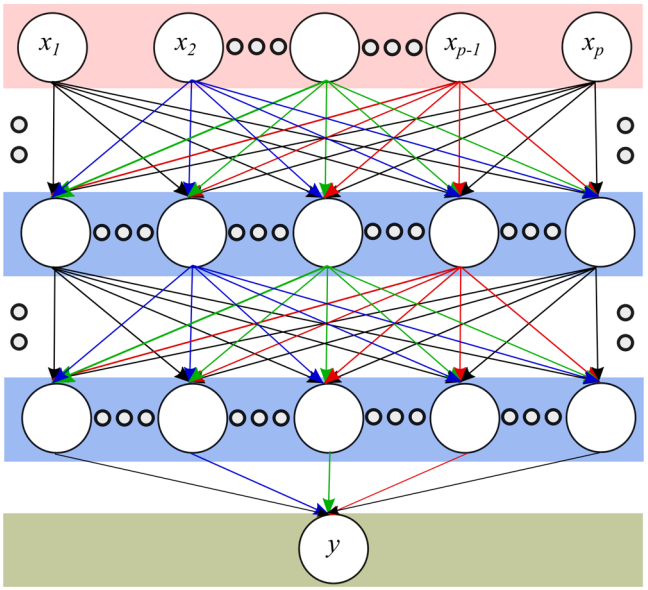

Figure 2. Simplified schematic of a neural network (NN). The top and bottom layer are the feature vector and output layer, respectively. Middle layers are the hidden layers. x_1, x_2,.....,x_p represent the features of the ML model. p represents the number of features and $y = \kappa_L$ is the final output.

the number of nodes in each hidden layer are chosen through careful experimentation such that we can avoid overfitting of the ML model. Indeed, the number of hidden layers and the number of nodes in each hidden layer are two main hyperparameters[36] that control the architecture of the NN, and they solely depend on the specific data set.

At the beginning of the training, the weights and biases of each link are chosen arbitrarily. In general, the initial weights and biases result in abysmal accuracy. The output from the nth node in the lth layer of the network is calculated as

$$f_{l,n} = \phi(\boldsymbol{x}^{l,n}\cdot\boldsymbol{w}^{l,n} + b_{l,n}) = \phi\left(\sum_{j=1}^{p} x_j^{l,n} w_j^{l,n} + b_{l,n}\right) \quad (4)$$

where j is the index of input, ϕ is the activation function, $\boldsymbol{x}$ is the input vector to the (l,n) node, $\boldsymbol{w}$ is the weight vector that contains the weight factors for each input to that particular node, p represents the number of inputs to the node, and b is the bias factor. For our study, we use scaled exponential linear activation function.[37] We choose to use the optimizer "Adam"[38] because it performs well with less tuning of the hyperparameters and requires a small amount of memory.

The training steps can be summarized as follows: (i) the assigned or adjusted weights and biases are used to calculate the output y from the feature vector $\boldsymbol{x}$. (ii) The errors, that is, the difference between the obtained output y, that is, κ_L and actual output $\hat{y}$ are calculated as $E = \hat{y} - y$. (iii) Through the backward propagation algorithm, the weight factor for each input of each node is adjusted. The details about the adjustments of weights through the backpropagation algorithm for the NN approach can be found in the ML textbooks.[36] Steps (i)−(iii) are repeated for sufficient epochs (N_{epochs}, a hyperparameter that defines the number of times the training algorithm works through the entire training data set) to obtain the desired accuracy. In particular, we choose N_{epochs} such that the mean absolute percentage error (MAPE) of κ_L for the validation data set (20% of the training data set) drops below ∼5% for each case, as reported in Section 3.3. Once we train the ML model for the selected number of epochs, we fix the weights and biases for each node. Then, these fixed weights and biases are used to calculate the final output for any input feature vector corresponding to RML structures that are not used for training. We implement our ML model using the open-source libraries of python.[39]

3. RESULTS AND DISCUSSIONS

3.1. Impact of Layer Thickness Arrangement on Thermal Conductivity of RMLs. In this section, we study the impact of the arrangement of layer thicknesses on the κ_L of RMLs. If the layer thicknesses of an RML are ordered in ascending order (Figure 1c), then the structure becomes a gradient multilayer (GML), which is a pseudo-RML. In fact, GML itself is one of the possible RMLs for a specific thickness distribution. To gradually make a GML more disordered, thus turning into an RML, we introduce disorder to its layer thicknesses by swapping the thicknesses of the randomly selected ith and jth layers of the same type of atom. Obviously, RMLs obtained in this way have the same thickness distribution as the starting GML, but they are different in the arrangement (order) of the thicknesses. We use the number of swaps (S) to quantify the introduced disorder in GML. Notably, S is not always the minimum number of swaps required to build an RML from its corresponding GML. Moreover, it is evident that swapping two layers with a larger distance might disorder the GML/RML structure more significantly than swapping two layers closer to each other. However, we note that, herein, S is merely used as a strategy for us to generate structures with approximately increasing disorder as testing structures for machine learning models, which turns out to suffice the purpose.

Here, we start from two GMLs (GML1 and GML2), both of which have $N = 32$ periods and an average thickness of $d = 4$ UC but have different thickness distributions. For each GML, we conduct 10 independent rounds of swappings to obtain 10 sets of RMLs with S varying from 0 (the original GML) to 50. Therefore, we will have 500 structures for each layer thickness distribution, that is, GML1 and GML2. The relations between κ_L and S are shown in Figure 3a (GML1) and Figure 3f (GML2). Obviously, κ_L decreases as S increases in GMLs.

https://dx.doi.org/10.1021/acsami.9b18084
ACS Appl. Mater. Interfaces 2020, 12, 8795−8804

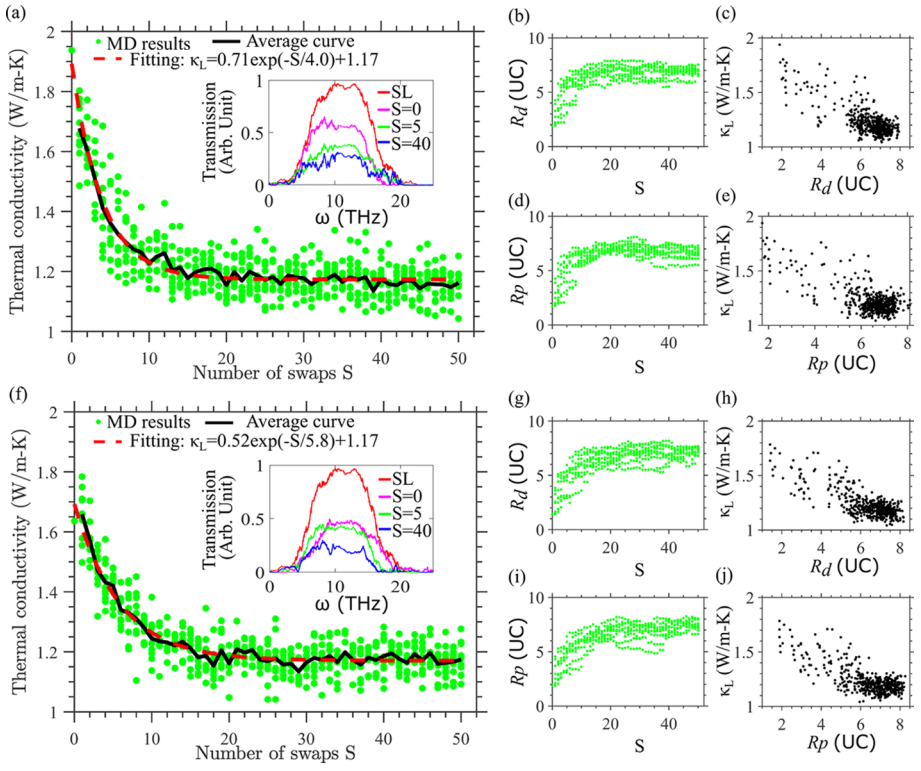

Figure 3. Changes of lattice thermal conductivity as GML is introduced with randomness through the thickness position swapping method for (a) GML1 and (f) GML2. For each S, we have 10 κ_L's because we have conducted the swapping method 10 times independently for each GML, and eventually, we obtained 10 sets of structures (each set has 50 RML structures). $S = 0$ signifies the unswapped GML. The insets of panels (a) and (f) are the normalized transmission spectra of SL, GML, RML ($S = 5$), and RML ($S = 40$), corresponding to GML1 and GML2, respectively. The transmission spectra are obtained from the same nonequilibrium molecular dynamics simulations in which we obtain the thermal conductivity data, and the normalization of transmission is done with respect to maximum transmission of SL. The changes of R_d with respect to the number of swaps are provided in (b) GML1 and (g) GML2. (c, h) Changes of κ_L with respect to R_d for GML1 (GML2). The changes of R_p with respect to the number of swaps are provided in (d) GML1 and (i) GML2. (e, j) Changes of κ_L with respect to R_p for GML1 (GML2).

Moreover, we note that κ_L decays exponentially as S increases. Specifically, we fit the data with $\kappa_L = ae^{-S/b} + c$ of which the fitting parameters are $a = 0.71$, $b = 4.0$, and $c = 1.17$ for GML1 and $a = 0.52$, $b = 5.8$, and $c = 1.17$ for GML2. The fitting curves almost overlaps with the averaged $\kappa_L - S$ curve, as shown in Figure 3a,f.

To quantify the randomness in layer thicknesses, we adopt the concept of thickness-based index of randomization R_d as[40]

$$R_d = \sqrt{\frac{\sum_{i=2}^{N}[(d_{A,i} - d_{A,i-1})^2 + (d_{B,i} - d_{B,i-1})^2]}{N}} \quad (5)$$

where $d_{A,i}$ and $d_{B,i}$ are the thickness of materials A and B in the ith period and N is the number of periods in RML. In fact, R_d is reported to be adequate to correlate the randomness of RML quantum wells with their photoluminescence.[40] R_d as a function of S is shown in Figure 3b (GML1) and Figure 3g (GML2), and it is evident that R_d increases as S increases. From Figure 3c and 3h, it can further be appreciated that the κ_L of GML1 (GML2) decreases as R_d increases, in general.

In addition to the randomness of thickness of successive layers, **period wise** randomness will also arise during the swapping procedure, that is, the nth period length can be significantly different from the $(n + 1)$th period length. To quantify the period wise randomness, we define the period-based index of randomness R_p as

$$R_p = \sqrt{\frac{\sum_{i=2}^{N}[((d_{A,i} + d_{B,i}) - (d_{A,i-1} + d_{B,i-1}))^2]}{N}} \quad (6)$$

Similar to R_d, R_p also increases as S increases, as shown in Figure 3d (GML1) and Figure 3i (GML2). Moreover, it is observed that κ_L decreases as R_p increases (Figure 3e,j), in general. Comparing Figure 3a–e (f–j) for GML1 (GML2), in which the reported κ_L's correspond to the RMLs with the same thickness distribution but different thickness arrangements, we can claim that R_d and R_p are the two effective, if not the only, parameters that can relate the κ_L's with the disorder of RMLs for a given thickness distribution. From Figure 3, we can further conclude that the swapping method can be helpful in obtaining an arrangement with a lower κ_L for a given thickness distribution.

We compare the normalized (with respect to the maximum transmission of the corresponding SL) phonon transmission of GML ($S = 0$) and two RMLs (with $S = 5$ and 40) in the inset of Figure 3a (GML1) and Figure 3f (GML2). In the same plots, we also report the phonon transmission of the corresponding SL with the same interface density and average layer thickness. From the transmission plots, we can reaffirm that, as opposed to an SL, a GML experiences a broadband phonon localization, and the localization effect becomes more dominant as we introduce disorder to a GML through the swapping method.

https://dx.doi.org/10.1021/acsami.9b18084
ACS Appl. Mater. Interfaces 2020, 12, 8795–8804

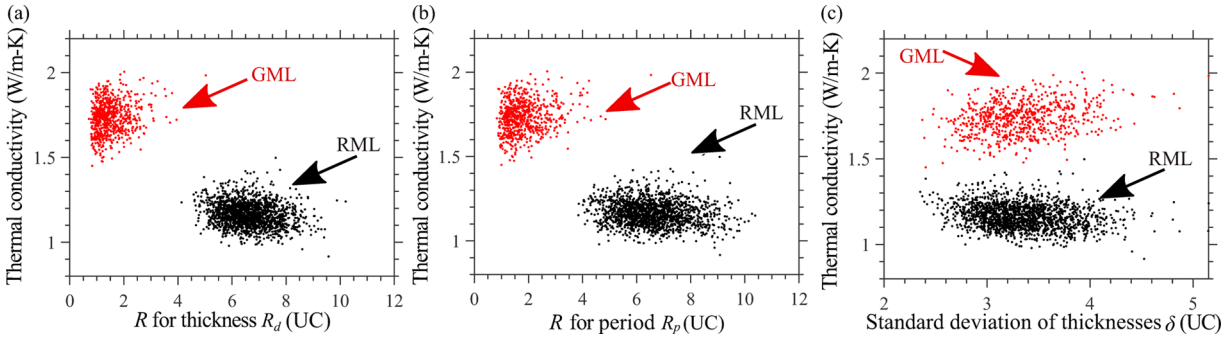

Figure 4. Changes of lattice thermal conductivity of 3400 multilayer structures with respect to the change of (a) R for layer thickness (R_d), (b) R for period (R_p), and (c) standard deviation of layer thicknesses (δ). Among the 3400 structures, 1700 structures are randomly generated RMLs, and the other 1700 structures are their corresponding GMLs.

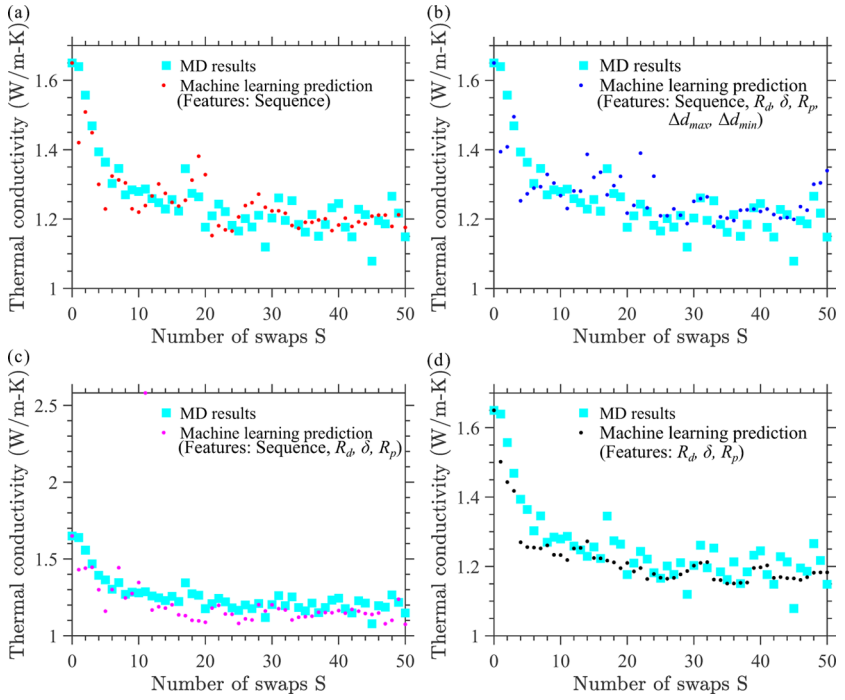

Figure 5. Comparison between MD-predicted thermal conductivity, that is, the true values, and ML-predicted values of a set of RMLs generated by the swapping method with S increasing from 0 (GML) to 50. The data used for training the ML model are the configurations and the corresponding MD-predicted thermal conductivities of 451 structures: one GML plus nine sets of RMLs generated through the swapping method, each of which containing 50 RMLs with the number of swaps S increasing from 1 to 50. Different combinations of parameters are used as the features for the ML model. Specifically, (a) sequence; (b) sequence, R_d, δ, R_p, Δd_{max}, and Δd_{min}; (c) sequence, R_d, δ, and R_p; and (d) R_d, δ, and R_p are used for training the model.

In general, we observe a decreasing trend of κ_L as S increases. The trend is not 100% monotonic, that is, in many cases, the κ_L of the structure obtained after Nth swaps is higher than that structure obtained after $(N-1)$th swaps. This increment may have arisen due to the formation of mini-superlattices (mini-SLs), that is, short length SLs within the RMLs, which facilitate the formation of coherent phonons. At this point of discussion, we want to mention that the κ_L of the corresponding SL ($N = 32$ and $d = 4$ UC) is obtained to be 3.7 W/(m·K). As expected, κ_L of SL is higher than both GMLs and RMLs.

So far, we have confined our discussions to the randomness and κ_L of RMLs for a given thickness distribution. Based on our findings, R_d and R_p are very effective for correlating the disorder with κ_L for different arrangements of RMLs with the same thickness distribution. However, to choose the best RML, that is, one with the lowest κ_L , we need to compare the κ_L of RMLs of different thickness distributions. We believe that R_d and R_p are not sufficient to distinguish between RMLs with different thickness distributions. Therefore, we will study RMLs with different thickness distributions in the following section.

3.2. Impact of Layer Thickness Distribution on Thermal Conductivity of RMLs. In this section, we strive to quantitatively correlate the disorder of RMLs of different thickness distributions with their κ_L. Thus, we generate 3400 multilayer structures with $N = 32$ and $d = 4$ UC, half of which are randomly generated RML structures and the other half are their corresponding GMLs. We conduct MD simulations to calculate the κ_L of these structures. The impact of N and d on κ_L of RMLs has already been studied in our earlier works.[11,30]

https://dx.doi.org/10.1021/acsami.9b18084
ACS Appl. Mater. Interfaces 2020, 12, 8795−8804

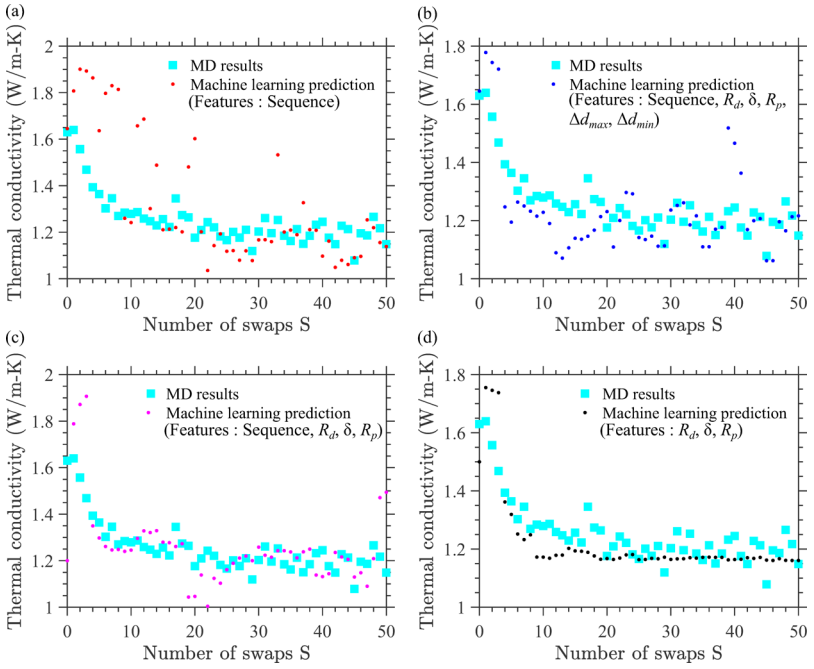

Figure 6. Comparison between MD-predicted thermal conductivity, that is, the true values, and ML-predicted values of a set of RMLs generated by the swapping method with S increasing from 0 (GML) to 50. The structural attributes and lattice thermal conductivity of 3400 multilayer structures (1700 of them are randomly generated RMLs, and the other 1700 are their corresponding GMLs) are used for training the ML model. Different combinations of parameters are used as the features for the ML model. Specifically, (a) sequence; (b) sequence, R_d, δ, R_p, Δd_{max}, and Δd_{min}; (c) sequence, R_d, δ, and R_p; and (d) R_d, δ, and R_p are used for training the model.

Therefore, we choose sufficiently large N and d to obtain a wide variation of disorder and κ_L of the RMLs.

We first report κ_L as a function of R_d and R_p in Figure 4a,b, respectively. Obviously, both R_d and R_p can distinguish between the κ_L of RMLs and the corresponding GMLs. However, as mentioned earlier, these two parameters do not consider the difference in thickness distribution explicitly. Thus, we need additional parameters to describe the differences between RMLs with different thickness distributions. Obviously, standard deviation (δ) is one of them, which is defined as

$$\delta = \sqrt{\frac{\sum_{i=1}^{N}[(d_{A,i} - d)^2 + (d_{B,i} - d)^2]}{2N}} \quad (7)$$

The δ of the 3400 structures and the corresponding κ_L's are shown in Figure 4c. As expected, δ cannot distinguish between the κ_L of an RML and its GML because they have the same thickness distribution. However, it is obvious that κ_L should depend on δ and there is a strong evidence to support this statement.[24] A careful inspection of Figure 4a,b and consideration of the findings by Juntunen et al.[24] help us conclude that the κ_L of an RML depends on R_d, R_p, and δ in a nonlinear and complex manner. Therefore, we believe that there are more relevant parameters that can help us quantitatively relate disorder with κ_L of RMLs more precisely.

So far, we can conclude that thickness distribution and thickness arrangement are the fundamental attributes that define the κ_L of an RML and that any statistical model should be able to predict the κ_L of RMLs if the model can distinguish among different thickness distributions and different arrangements for a specific thickness distribution. A machine learning (ML) model could be a powerful tool that can handle the complexity of the problem if we can adequately feed the ML model with the structural information and the corresponding κ_L of RMLs.

3.3. Machine Learning-Based Prediction of κ_L. We first adopt the ML model to predict the κ_L of different arrangements of an RML. In particular, we choose a GML and generate 10 sets of RMLs from the GML through the swapping method and calculate their κ_L using MD simulations. Details of the thickness swapping method can be found in Section 3.1.

Nine sets of the data (out of the 10 sets that we generated) are used for training the ML model, and the 10th one is used for testing the model. Each set has 50 RML structures, and accordingly, our training (testing) set consists of 450 (50) RML structures and their κ_L. The training sample with 450 data may seem a small quantity. However, all the considered structures (generated through the swapping method) have the same thickness distribution, and the difference among them is just the thickness arrangement. Therefore, 450 training data are found to be sufficient for training the ML model. We consider the thickness sequence, R_d, R_p, δ, Δd_{max}, and Δd_{min} as the features for the ML model where Δd_{max} and Δd_{min} represent the maximum and minimum deviation of layer thickness with respect to the mean layer thickness of RML, as defined in ref 24. The predicted κ_L's of the RMLs from the ML model are compared with the actual value from MD simulations in Figure 5.

We test the performance of four different combinations of features: (i) layer thickness sequence (Figure 5a); (ii) layer thickness sequence, R_d, δ, R_p, δ, Δd_{max}, and Δd_{min} (Figure 5b); (iii) layer thickness sequence, R_d, δ, and R_p (Figure 5c); and (iv) R_d, δ, and R_p (Figure 5d). From Figure 5, it is obvious that the ML model predicts the decreasing trend of κ_L of RMLs reasonably well for all the four types of combinations. From Figure 5a, we can conclude that the thickness sequence is a

https://dx.doi.org/10.1021/acsami.9b18084
ACS Appl. Mater. Interfaces 2020, 12, 8795−8804

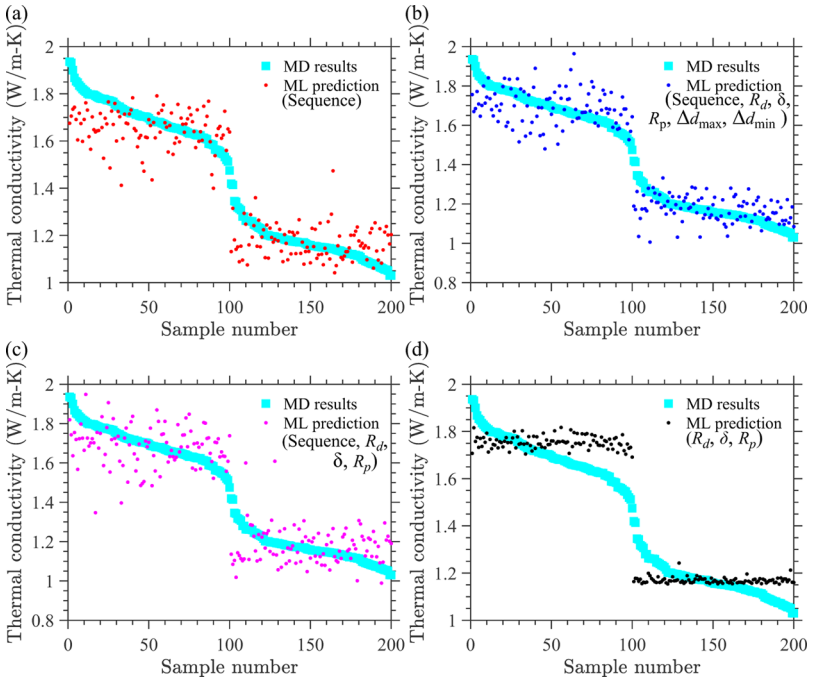

Figure 7. Machine learning prediction of lattice thermal conductivity of 200 multilayer structures (100 of them are randomly generated RMLs, and the other 100 are their corresponding GMLs) for different combination of features: (a) sequence, (b) sequence, R_d, δ, R_p, Δd_{max}, and Δd_{min}; (c) sequence, R_d, δ, and R_p; and (d) R_d, δ, and R_p. To aid the visualization, we represent the GMLs with sample numbers 1−100, and we represent the corresponding RMLs with sample numbers 101−200. Moreover, the data points are arranged in order of decreasing actual (MD) thermal conductivity along the horizontal axis for a better visualization of the data. The features, used for training and testing, in the ML model are provided in each plot just below the legend. The structural attributes and thermal conductivity of 3200 multilayer structures (1600 of them are RMLs, and the other 1600 are their corresponding GMLs) are used for training the ML model.

sufficient feature for an ML model to predict the κ_L of RMLs with different arrangements but the same thickness distribution. The ML model is observed to predict the κ_L of ∼80% structures with an error percentage of less than 15%. If the sequence is assisted with other parameters like R_d, δ, R_p, Δd_{max}, or Δd_{min}, then the accuracy does not seem to improve (Figure 5b,c). More interestingly, the disorder parameters identified by us (R_d, δ, and R_p) are found to be self-sufficient features for an ML to predict the decreasing trend of κ_L with reasonable accuracy (Figure 5d). This indeed provides a more efficient approach than using the thickness sequence as the feature. Specifically, the thickness sequence has $2 \times N$ (64 for our study) elements, which makes the training and testing process slow. On the other hand, R_d, R_p, δ, Δd_{max}, and Δd_{min} compress the structural information of an RML, so the ML model will deal with less elements and therefore performs faster. Thus, we would claim that we have identified a few key parameters (R_d, R_p, δ, Δd_{max}, and Δd_{min}) that are important for an ML model to effectively predict the κ_L of RMLs with different arrangement of thickness and the same thickness distribution.

So far, we have used the data from the swapping method for both training and testing the ML model. To make our model more generic, we change our training samples to increase the difficulty level of the ML model for predicting κ_L. In particular, we train the ML model with the features κ_L data of 3400 sets of multilayer structures (1700 of them are RMLs, and the other 1700 are their corresponding GMLs) with random thickness distribution. Then, we use this model to predict the κ_L of the testing structures in Section 3.3 and Figure 5. The results are presented in Figure 6 alongside the actual MD values.

From Figure 6a, we can conclude that the thickness sequence alone is not a sufficient feature to predict the κ_L of RMLs with reasonable quantitative accuracy, at least in the high κ_L regime. In other words, the sequence does not appear to be a sufficient feature to predict the κ_L of RMLs with different thickness distributions. However, the identified disorder parameters (R_d, δ, and R_p) can aid the prediction once they are used as features along with the thickness sequence, as shown in Figure 6b,c. It is worth noting that the identified disorder parameters themselves seem to be sufficient to distinguish the κ_L of different arrangements of RML for a given thickness distribution (Figure 6d). Even though the ML-predicted κ_L smears out to be a constant value after a certain number of swaps, these disorder parameters would be sufficient to predict the general decreasing trend of κ_L and help screen out the RMLs with high κ_L. All in all, we conclude that the sequence, R, δ, and R_p are crucial features to obtain an accurate prediction of κ_L of RMLs with uncontrolled thickness distribution from an ML model.

Finally, to make the ML model more general, we train it with the features κ_L data of 3200 randomly generated multilayer structures (1600 are RMLs, and the other 1600 are their corresponding GMLs) and predict the κ_L of another 200 randomly generated multilayers (100 are RMLs, and the other 100 are their corresponding GMLs). The ML-predicted κ_L for the 200 structures are displayed in Figure 7. Evidently, the ML model can distinguish between the κ_L of GMLs and the corresponding RMLs for all of the feature vectors considered in our study. From Figure 7a−c, we can conclude that thickness sequence R_d, δ, R_p, Δd_{max}, and Δd_{min} are all indeed very important (if not the only) features to predict the κ_L of RMLs. However, the thickness sequence plays the most important role in an ML model to distinguish among multilayer structures. If we just use R_d, δ, and R_p as the

https://dx.doi.org/10.1021/acsami.9b18084
ACS Appl. Mater. Interfaces 2020, 12, 8795−8804

features, then the ML model can still distinguish between the GMLs and RMLs (Figure 7d). However, ML predicts almost the same κ_L for different GMLs (or RMLS).

In conclusion, the thickness sequence is a crucial feature for an ML model to predict the κ_L of RMLs accurately, especially when they have various thickness distributions. Moreover, the identified disorder parameters assist in obtaining a better prediction. However, we note that, even though ML can help us predict κ_L, it cannot reveal the underlying physics, at least not explicitly. Considering the high computational cost of MD simulations, ML can be a very powerful tool for estimating the κ_L of numerous structures using limited simulation results (for training the ML model), which could be very useful for high-throughput screening of the layer thickness distribution and arrangement to obtain the lowest κ_L.

4. CONCLUSIONS

We have identified more effective parameters than conventional ones to quantify the disorder in the layer thicknesses of random multilayer (RML) structures, and we were able to correlate these parameters with the lattice thermal conductivity of RMLs successfully. Moreover, we have shown that machine learning can be an effective tool for screening for the optimal thickness distribution and thickness arrangement. We have revealed that thickness-based index of randomization (eq 5), period-based index of randomization (eq 6), and the standard deviation (eq 7) are essential features for a machine learning model to predict the lattice thermal conductivity of RMLs more accurately and more efficiently. The thickness sequence can also perform well as a feature if the number of training data is high. This work will be important for the development of multilayer structures with ultralow thermal conductivity and the search for structures with strong phonon Anderson localization, which is a burgeoning research field.[22,30,33,41−43]

AUTHOR INFORMATION

Corresponding Authors

Run Hu − *School of Energy and Power Engineering, Huazhong University of Science and Technology, Wuhan 430074, China;* orcid.org/0000-0003-0274-9982; Phone: +86-135-5423-4060; Email: hurun@hust.edu.cn

Yan Wang − *Department of Mechanical Engineering, University of Nevada, Reno, Reno, Nevada 89557, United States;* orcid.org/0000-0001-9474-6396; Phone: +1775-784-6468; Email: yanwang@unr.edu; Fax: (775) 784-1390

Authors

Pranay Chakraborty − *Department of Mechanical Engineering, University of Nevada, Reno, Reno, Nevada 89557, United States*

Yida Liu − *School of Energy and Power Engineering, Huazhong University of Science and Technology, Wuhan 430074, China*

Tengfei Ma − *Department of Mechanical Engineering, University of Nevada, Reno, Reno, Nevada 89557, United States*

Xixi Guo − *Department of Mechanical Engineering, University of Nevada, Reno, Reno, Nevada 89557, United States*

Lei Cao − *Department of Mechanical Engineering, University of Nevada, Reno, Reno, Nevada 89557, United States*

Complete contact information is available at: https://pubs.acs.org/10.1021/acsami.9b18084

Notes

The authors declare no competing financial interest.

ACKNOWLEDGMENTS

P.C., T.M., X.G., L.C., and Y.W. thank the University of Nevada, Reno for the faculty startup fund and the NASA EPSCoR Research Infrastructure Development grant (no. NNX15AK48A). The authors acknowledge the support from the Information Technology Department at the University of Nevada, Reno for computing time on the Pronghorn (a high-performance computing (HPC) cluster). P.C. acknowledges Rahul Dubey and Raj Shukla, both from the Computer Science Department of University of Nevada, Reno, for the important discussions on machine learning.

REFERENCES

(1) Smialek, J. L.; Miller, R. A. Revisiting the Birth of 7YSZ Thermal Barrier Coatings: Stephan Stecura. *Coatings* **2018**, *8*, 255.

(2) Zhu, D. Advanced Environmental Barrier Coatings for SiC/SiC Ceramic Matrix Composite Turbine Components. *Eng. Ceram.* **2016**, 187−202.

(3) Zhu, D.; Miller, R. A. Development of Advanced Low Conductivity Thermal Barrier Coatings. *Int. J. Appl. Ceram. Technol.* **2004**, *1*, 86−94.

(4) Blackburn, J. L.; Ferguson, A. J.; Cho, C.; Grunlan, J. C. Carbon-Nanotube-Based Thermoelectric Materials and Devices. *Adv. Mater.* **2018**, *30*, 1704386.

(5) Chakraborty, P.; Ma, T.; Zahiri, A. H.; Cao, L.; Wang, Y. Carbon-based Materials for Thermoelectrics. *Adv. Condens. Matter Phys.* **2018**, *2018*, 1.

(6) Liao, B.; Chen, G. Nanocomposites for Thermoelectrics and Thermal Engineering. *MRS Bull.* **2015**, *40*, 746−752.

(7) Snyder, G. J.; Toberer, E. S. Complex Thermoelectric Materials. *Nat. Mater.* **2008**, *7*, 105−114.

(8) Alam, H.; Ramakrishna, S. A review on the Enhancement of Figure of Merit from Bulk to nano-Thermoelectric Materials. *Nano Energy* **2013**, *2*, 190−212.

(9) Borland, J.; Dawkins, P.; Johnson, D.; Williams, R. *SPACE EXPLORATION: DOE Could Improve Planning and Communication Related to Plutonium-238 and Radioisotope Power Systems Production Challenges*; U.S. Government Accountability Office, 2017.

(10) United States. General Accounting Office *Space Exploration : Power Sources for Deep Space Probes : Report to the Honorable Barbara Boxer, U.S. Senate*; The Office, 1998.

(11) Wang, Y.; Gu, C.; Ruan, X. Optimization of the Random Multilayer Structure to Break the Random-Alloy Limit of Thermal Conductivity. *Appl. Phys. Lett.* **2015**, *106*, No. 073104.

(12) Hicks, L. D.; Dresselhaus, M. S. Effect of Quantum-well Structures on the Thermoelectric Figure of Merit. *Phys. Rev. B* **1993**, *47*, 12727.

(13) Hicks, L. D.; Dresselhaus, M. S. Thermoelectric Figure of Merit of a One-Dimensional Conductor. *Phys. Rev. B* **1993**, *47*, 16631.

(14) Hochbaum, A. I.; Chen, R.; Delgado, R. D.; Liang, W.; Garnett, E. C.; Najarian, M.; Majumdar, A.; Yang, P. Enhanced Thermoelectric Performance of Rough Silicon nanowires. *Nature* **2008**, *451*, 163.

(15) Venkatasubramanian, R.; Siivola, E.; Colpitts, T.; O'Quinn, B. Thin-film Thermoelectric Devices with High Room-Temperature Figures of Merit. *Nature* **2001**, *413*, 597.

(16) Biswas, K.; He, J.; Blum, I. D.; Wu, C.-I.; Hogan, T. P.; Seidman, D. N.; Dravid, V. P.; Kanatzidis, M. G. High-Performance Bulk Thermoelectrics with all-scale Hierarchical Architectures. *Nature* **2012**, *489*, 414.

(17) Harman, T. C.; Taylor, P. J.; Walsh, M. P.; LaForge, B. E. Quantum Dot Superlattice Thermoelectric Materials and Devices. *Science* **2002**, *297*, 2229−2232.

(18) Liu, W.; Yan, X.; Chen, G.; Ren, Z. Recent Advances in Thermoelectric nanocomposites. *Nano Energy* **2012**, *1*, 42−56.

(19) Finefrock, S. W.; Wang, Y.; Ferguson, J. B.; Ward, J. V.; Fang, H.; Pfluger, J. E.; Dudis, D. S.; Ruan, X.; Wu, Y. Measurement of

Thermal Conductivity of pbte Nanocrystal Coated Glass Fibers by the 3ω Method. *Nano Lett.* **2013**, *13*, 5006−5012.
(20) Böttner, H.; Chen, G.; Venkatasubramanian, R. Aspects of Thin-film Superlattice Thermoelectric Materials, Devices, and Applications. *MRS Bull.* **2006**, *31*, 211−217.
(21) Tritt, T. M.; Subramanian, M. A. Thermoelectric Materials, Phenomena, and Applications: a Bird's Eye View. *MRS Bull.* **2006**, *31*, 188−198.
(22) Wang, Y.; Huang, H.; Ruan, X. Decomposition of Coherent and Incoherent Phonon Conduction in Superlattices and Random Multilayers. *Phys. Rev. B* **2014**, *90*, 165406.
(23) Qiu, B.; Chen, G.; Tian, Z. Effects of Aperiodicity and Roughness on Coherent Heat conduction in Superlattices. *Nanoscale Microscale Thermophys. Eng.* **2015**, *19*, 272−278.
(24) Juntunen, T.; Vänskä, O.; Tittonen, I. Anderson Localization Quenches Thermal Transport in Aperiodic Superlattices. *Phys. Rev. Lett.* **2019**, *122*, 105901.
(25) Hu, L.; Schmidt, A.; Narayanaswamy, A.; Chen, G. Effects of Periodic Structures on the Coherence Properties of Blackbody Radiation. *J. Heat Transfer* **2004**, *126*, 786−792.
(26) Ruan, X. L.; Kaviany, M. Photon Localization and Electromagnetic Field Enhancement in Laser-irradiated, Random Porous Media. *Microscale Thermophys. Eng.* **2005**, *9*, 63−84.
(27) Ma, T.; Liang, C.; Wang, L.-G.; Lin, H.-Q. Electronic Band Gaps and Transport in Aperiodic Graphene Superlattices of Thue-Morse Sequence. *Appl. Phys. Lett.* **2012**, *100*, 252402.
(28) Wu, Y.-J.; Fang, L.; Xu, Y. Predicting Interfacial Thermal Resistance by Machine Learning. *npj Comput. Mater.* **2019**, *5*, 56.
(29) Oliynyk, A. O.; Antono, E.; Sparks, T. D.; Ghadbeigi, L.; Gaultois, M. W.; Meredig, B.; Mar, A. High-throughput Machine-learning-driven Synthesis of full-Heusler Compounds. *Chem. Mater.* **2016**, *28*, 7324−7331.
(30) Chakraborty, P.; Cao, L.; Wang, Y. Ultralow Lattice Thermal Conductivity of the Random Multilayer Structure with Lattice Imperfections. *Sci. Rep.* **2017**, *7*, 8134.
(31) Ju, S.; Shiga, T.; Feng, L.; Hou, Z.; Tsuda, K.; Shiomi, J. Designing nanostructures for phonon transport via Bayesian optimization. *Phys. Rev. X* **2017**, *7*, No. 021024.
(32) Chen, Y.; Li, D.; Lukes, J. R.; Ni, Z.; Chen, M. Minimum Superlattice Thermal Conductivity from Molecular Dynamics. *Phys. Rev. B* **2005**, *72*, 174302.
(33) Wang, Y.; Vallabhaneni, A.; Hu, J.; Qiu, B.; Chen, Y. P.; Ruan, X. Phonon Lateral Confinement Enables Thermal Rectification in Asymmetric Single-Material nanostructures. *Nano Lett.* **2014**, *14*, 592−596.
(34) Plimpton, S. Fast Parallel Algorithms for Short-range Molecular Dynamics. *J. Comput. Phys.* **1995**, *117*, 1−19.
(35) Sääskilahti, K.; Oksanen, J.; Volz, S.; Tulkki, J. Frequency-dependent phonon mean free path in carbon nanotubes from nonequilibrium molecular dynamics. *Phys. Rev. B* **2015**, *91*, 115426.
(36) Haykin, S. *Neural Networks: A Comprehensive Foundation*; 1st Ed.; Prentice Hall PTR: Upper Saddle River, NJ, USA, 1994.
(37) Klambauer, G.; Unterthiner, T.; Mayr, A.; Hochreiter, S. In *Advances in Neural Information Processing Systems 30*; Guyon, I.; Luxburg, U. V.; Bengio, S.; Wallach, H.; Fergus, R.; Vishwanathan, S.; Garnett, R. Eds.; Curran Associates, Inc., 2017; pp 971−980.
(38) Kingma, D. P.; Ba, J. Adam: A Method for Stochastic Optimization. *arXiv preprint arXiv:1412.6980* 2014.
(39) Chollet, F. *Keras*. https://keras.io , 2015.
(40) Shih, Y. C. A.; Sadra, K.; Streetman, B. Random-period Superlattice Quantum Wells. *J. Vac. Sci. Technol., B: Microelectron. Nanometer Struct.–Process., Meas., Phenom.* **1994**, *12*, 1082−1085.
(41) Luckyanova, M. N.; Mendoza, J.; Lu, H.; Song, B.; Huang, S.; Zhou, J.; Li, M.; Dong, Y.; Zhou, H.; Garlow, J.; Wu, L.; Kirby, B. J.; Grutter, A. J.; Puretzky, A. A.; Zhu, Y.; Dresselhaus, M. S.; Gossard, A.; Chen, G. Phonon localization in heat conduction. *Sci. Adv.* **2018**, *4*, eaat9460.
(42) Mendoza, J.; Chen, G. Anderson Localization of Thermal Phonons Leads to a Thermal Conductivity Maximum. *Nano Lett.* **2016**, *16*, 7616−7620.
(43) Tian, Z. Anderson Localization for Better Thermoelectrics? *ACS Nano* **2019**, *13*, 3750−3753.

https://dx.doi.org/10.1021/acsami.9b18084
ACS Appl. Mater. Interfaces 2020, 12, 8795−8804